International Journal of Microwave and Wireless Technologies, 2013, 5(4), 537–550.
doi:10.1017/S1759078713000196

RESEARCH PAPER

Electrodynamic analysis of nanoantennas at millimeter and optical wavelength ranges

ALEXANDER M. LERER, ELENA V. GOLOVACHEVA, ANATOLY B. KLESHCHENKOV, GENNADY A. SHUROV, PAVEL V. MAKHNO AND VICTORIA V. MAKHNO

Electrodynamics models and radiophysical properties of carbon nanotube-dipoles (isolated on the substrate lattices), metallic optical antennas and optical antennas, formed from ZnO nanorods coated with metal films were developed and investigated. The models are based on numerically analytical solution of integrodifferential equations describing the diffraction of electromagnetic waves on impedance and dielectric bodies. The use of integral representations of the kernels of integrodifferential equations allowed us to overcome the difficulties of solution, associated with the singularity of kernels and to reduce the computation time by an order of magnitude.

Keywords: EM field theory and numerical techniques, Antenna design, Modeling and measurements

Received 27 July 2012; Revised 6 February 2013; first published online 3 April 2013

I. INTRODUCTION

It is well known that conductance of a typical wire is inversely proportional to its length and its cross-section. Charge transport in carbon nanotubes (CNTs) has a quantum nature [1]. CNT's conductance does not depend on its length or thickness and is equal to the so-called quantum conductance – limit value of conductivity, corresponding to free electron transport along the whole length of conductor. The electroconductivity of nanotubes is higher than electroconductivity of all known conductors of similar sizes and the value of current density in conducting nanotube, observed at normal temperature and is of two orders higher than that presently obtained in superconductors.

If we consider nanotubes as transmission lines, we can outline some specialties that distinguish nanotubes from traditional transmission lines. For CNTs there is the notion of kinetic induction, whose value is much higher than traditional magnetic induction. Besides electrostatic capacity, it is necessary to take into account quantum capacity [1]. Hence, the speed of the wave's propagation in CNT is comparable to Fermi speed and not the speed of light c, and is equal to about $0.02c$. Thus, the wavelength in the nanotube is much smaller than the wavelength in the macroscopic metallic conductor. Therefore, resonant frequencies of a nanotube-dipole are much smaller than those for metallic dipole. A strong deceleration of the surface waves in nanotubes was first described in the [2]. For the first time, a rigorous theory of nanotubes–nanoantennas was constructed independently in [3, 4].

In [5, 6], the method for calculating the properties of the CNT-dipoles on the substrate was developed. This method was based on the solution of pair integral equations (PIEs) about Fourier transform of current density on a dipole. In this case, kernel singularity of integrodifferential equations (IDE) about the current on the dipole is transferred to the slow decrease of the integrand in the Fourier integral. To improve the convergence of the Fourier integral is easier than regularizing the IDE. For a dipole on a substrate, solution of PIE is preferable than solution of IDE because of the Green function (GF) expressed through the Fourier integral.

In conventional optics, light is usually controlled by redirection of wave fronts propagating radiation with the help of lenses, mirrors, and diffractive elements. This type of control is based on the wave nature of electromagnetic fields and, thus, is not applicable to guiding the fields in subwavelength scale, as opposed to radio and microwave bands, where antennas are used to control the fields in subwavelength scale and are an effective interface between the propagating radiation and localized fields. The same is true for the optical antenna (OA).

The properties of OAs are similar to antennas of radio frequency bands with some important differences in physical characteristics and non-fulfillment of the principle of scalability. The majority of differences are because the metal in the optical frequency range is not a perfect conductor, it has the properties of solid-state plasma, stipulated by the presence of free electron gas. Therefore, when solving problems of diffraction of electromagnetic waves in the optical frequency range on a metallic object, it is necessary to take into account the field inside the sample. OAs are used to increase the efficiency of energy transport from external field to local field and backwards. In the problems of microscopy, OA

Southern Federal University, Zorge Street, 5, Rostov-on-Don, 344090, Russian Federation. Phone: +7 863 297-51-29
Corresponding author:
A.M. Lerer
Email: lerer@sfedu.ru

replaces conventional focusing lenses or objectives allowing concentration on radiation in space dimensions smaller than the diffraction limit [7–9]. OA leads to a giant increase of local electric field. This property of OA can be used for increasing efficiency of photophysical processes in light-emitting devices and solar cells, determining DNA structure, and detection of separate molecules [7–9]. Similar to OA, CNTs [10], metal and metal dielectric dipoles, and spheres [11–15] are used.

There are several types of integral equations (IEs) describing diffraction on dielectric bodies. Most of these equations can be divided into two groups – surface IEs (SIEs) and volume IEs (VIEs). In the SIE, the unknown variable is the field at the interface between dielectrics. In the VIE, the unknown variable is the field at all internal points of the body. VIEs have several advantages: they are simpler, heterogeneous and the nonlinearity of the dielectric does not significantly complicate the solution and as a result the electric field in the dielectric is found. Applications of IEs for plasmonic structures are described in [15–18].

In the present work, the efficient numerical analytical method is applied to the diffraction problem of electromagnetic waves on metal-dielectric nanostructures [17]. To simulate the OA, formed by a system of N planar rectangular metal dipoles, arranged on the surface of the dielectric substrate, approximate boundary conditions (ABCs) for a thin dielectric layer are used. These ABCs take into account a finite value of the dielectric constant of metals in the optical range [18].

Presently, the core-shell structures based on ZnO nanorods coated with metal films are being developed. They can be used as nanoantennas in the visible and infrared ranges. The grids of such nanorods, coated with metallic films, may be grown at conducting sublayers, required for excitation of the plasmons.

Nanoelectromagnetism is based on consolidation of microscopy quantum theory of electron properties of nanostructures and classical macroscopic electrodynamics. In the present work, the following electromagnetic models are used:

(1) Quantum-mechanical properties of CNT in the model are described by macroscopic parameter–surface impedance.
(2) While investigating metallic nanowaveguides, diffraction gratings, and nanodipoles, the finite values of dielectric permittivity of metals in the optical frequency range were taken into account.

The objects of investigation in the present work are:

- CNT-dipoles (isolated; on the substrate; system of nanodipoles);
- metallic OA (round and elliptical profile; planar; lying on the substrate);
- OA, formed from ZnO nanorods coated with metal films.

II. CNT-DIPOLES

CNT grown by means of common technology are located normally to the substrate. We are analyzing the method of computing diffraction characteristics of N CNT-dipoles located normally at the substrate in random order. In this work, we are analyzing CNTs arranged in dielectric with dielectric permeability ε_1 normal to a dielectric substrate ε_2, $\mu_1 = \mu_2 = 1$. We introduce a rectangular coordinate system with X, Y axes parallel to the substrate and normal to CNT and Z-axis directed along the dipole and normal to the substrate. The origin of coordinates is lying on the substrate. The length of the CNT is L and radius is a.

We consider that the following boundary condition is correct on the surface of the dipole:

$$E_z = \rho_S j, \tag{1}$$

where E_z, j are the longitudinal components of electric field intensity and surface current density, ρ_S is the surface resistance of CNT [3, 4], $\rho_s = i(\pi^2 a\hbar(\omega - i\nu)/2e^2\upsilon_F)$, υ_F is the Fermi velocity (for CNT $\upsilon_F = 9.71 \times 10^5$ m/s), ω is the cyclic frequency, ν is the relaxation frequency (for CNT $\nu = 3.33 \times 10^{11}$Hz), e is the electron charge, c is the velocity of light in free space, and $\hbar$ is the Planck constant.

At first, we analyze a single CNT-dipole. We consider that only a longitudinal component of the current exists on the dipole and depends only on z. We use boundary condition (1). As a result, we derive the following expression:

$$\frac{1}{i\omega\varepsilon_1\varepsilon_0}\left(\frac{d^2}{dz^2} + k_1^2\right)\int_0^L j(z')g_e(z, z')dz' + E_z^e(z), \\ = \rho_s j(z),\ z \in [0,\ L] \tag{2}$$

where k_1 is the wave number in upper dielectric, the core of the IDE $g_e(z, z')$ is defined below.

We consider external field $E_z^e(z)$ as the sum of two plane waves – incident wave and wave reflected from the substrate without dipole. The reflection coefficient is defined by the Fresnel formula. The vector of $\vec{E}^e(z)$ is in the plane of incidence.

The kernel of the IDE

$$g_e(z, z') = \frac{a}{2\pi}\int_0^{2\pi} d\phi \int_0^{2\pi} g(x, x', y, y', z, z')d\phi'. \tag{3}$$

In expression (3), we consider that the observation point and the source point are lying on the surface of the dipole:

$$x = a\cos\phi,\ y = a\sin\phi,\ x' = a\cos\phi',\ y' = a\sin\phi'. \tag{4}$$

In expression (3), the function$g(x, x', y, y', z, z')$ is the GF for the vector potential in case the current direction is normal to the surface:

$$\left(\frac{\partial^2}{\partial x^2} + \frac{\partial^2}{\partial y^2} + \frac{\partial^2}{\partial z^2} + k^2\varepsilon\right)g(x, x', y, y', z, z') \\ = -\delta(x - x')\delta(y - y')\delta(z - z'). \tag{5}$$

Let $z' \geq 0$. For $z \geq 0$ we will retrieve the solution of (5) in the following form:

$$g(x, x', y, y', z, z') = \frac{1}{8\pi^2}\int_{-\infty}^{\infty}\int_{-\infty}^{\infty}\left[e^{-\gamma_1|z-z'|} + Q(\rho)\, e^{-\gamma_1(z+z')}\right] \\ \times \frac{1}{\gamma_1}e^{i\alpha\bar{x}+i\beta\bar{y}}d\alpha d\beta. \tag{6}$$

Following notations are used here and further $\bar{x} = x - x'$, $\bar{y} = y - y'$, $\gamma_{1,2} = \sqrt{\rho^2 - k_{1,2}^2}$, $\rho = \sqrt{\alpha^2 + \beta^2}$, k_2 is the wave number in the substrate, $Q = \gamma_1 - \gamma_2 t/\gamma_1 + \gamma_2 t$, $t = \varepsilon_1/\varepsilon_2$.

https://doi.org/10.1017/S1759078713000196 Published online by Cambridge University Press

The first term in (6) is a partial solution of an inhomogeneous equation (5) or in other words it is free-space GF:

$$g_0(x, x', y, y', z, z') = \frac{e^{-ik_1 R}}{4\pi R}.$$

The following integral representation is valid for it:

$$\frac{e^{-ik_1 R}}{4\pi R} = \frac{1}{4\pi^2}\int_{-\infty}^{\infty} K_0\left(R_1\sqrt{\rho^2 - k_1^2}\right)e^{-i\rho(z-z')}d\rho, \qquad (7)$$

where K_0 is the Macdonald function.

The second term includes the substrate influence. For $\varepsilon_1 = \varepsilon_2$, $g_1 = 0$:

$$g_2(x, x', y, y', z, z') = \frac{1}{8\pi^2}\int_{-\infty}^{\infty}\int_{-\infty}^{\infty} Q(\rho)\, e^{-\gamma_1(z+z')}\frac{1}{\gamma_1}e^{i\alpha\bar{x}+i\beta\bar{y}}d\alpha d\beta \qquad (8)$$

We substitute expressions (7) and (8) in (3), taking into account (4) and making the change of variables $\alpha = \rho\cos\vartheta$, $\beta = \rho\sin\vartheta$. As a result we obtain the following equation:

$$g_e(z, z') = g_{e,1}(z, z') + g_{e,2}(z, z'), \qquad (9)$$

$$g_{e,1}(z, z') = \frac{a}{2\pi}\int_{-\infty}^{\infty} I_0(a\gamma_1)K_0(a\gamma_1)e^{-i\rho(z-z')}d\rho, \qquad (10)$$

$$g_{e,2}(z, z') = \frac{a}{2\pi}\int_{0}^{\infty} \rho\, Q(\rho)\,\frac{e^{-\gamma_1(z+z')}}{\gamma_1}J_0^2(\rho a)\, d\rho, \qquad (11)$$

J_0 is the Bessel function, I_0 is the modified Bessel function.

We retrieve the solution of (2) using the Galerkin method

$$j(z) = \sum_{n=0}^{\infty} X_n\, V_n(z), \qquad (12)$$

X_n is the unknown coefficient, $V_n(z)$ is the basis function, in whose capacity we use weighted Chebyshev polynomials of the second order:

$$V_n(z) = \frac{i^n}{\pi(n+1)}\sqrt{1 - z^2/l^2}\, U_n\left(\frac{z}{l}\right), \quad n = 0, 1, 2\ldots. \qquad (13)$$

Fourier transformation of $V_n(z)$is expressed in terms of Bessel functions $\tilde{V}_n(\gamma) = J_{n+1}(\gamma l)/\gamma$. Substituting the current from (12) into (2) and then projecting equation (2) onto $V_p^*(z)$ we obtain the system of linear algebraic equations (SLAE):

$$\sum_{n=0}^{\infty} X_n\, A_{pn} = B_p,\ p = 0, 1\ldots,$$

with matrix elements A_{pn} in left and B_p in right parts:

$$A_{pn}(\rho) = \int_0^L dz V_p^*(z)\left(\frac{d^2}{dz^2} + k_1^2\right)\int_0^L V_n(z')g_e(\rho, z, z')dz', \qquad (14)$$

$$B_p = \frac{ik\varepsilon_1}{Z_c}\int_{-l}^{l} E^e(z)V_p^*(z)dz.$$

Matrix elements (14) of the retrieved SLAE are double integrals with kernels $g_e(\rho, z, z')$ that have singularity if $z = z'$. Using integral representation of the core (9), (10) we obtain the following expression after substitution expressions (9)–(11) in (4):

$$A_{pn} = A_{pn}^{(1)} + A_{pn}^{(2)} + A_{pn}^{(3)},$$

where

$$A_{pn}^{(1)} = \frac{\zeta_{pn}a}{\pi}\int_0^{\infty} \gamma_1^2 I_0(a\gamma_1)K_0(a\gamma_1)J_{p+1}(\rho l)J_{n+1}(\rho l)/\rho^2 d\rho, \qquad (15)$$

$$A_{pn}^{(3)} = \eta\int_{-l}^{l} V_p^*(z)\, V_n(z)dz = i\zeta_{nj}\frac{l}{\pi^2(p+1)(n+1)} \times \cos\frac{q\pi}{2}\left(\frac{1}{(p+n+2)^2-1} - \frac{1}{(p-n)^2-1}\right),$$

$\zeta_{pn} = 1$ if p, n of the same parity, otherwise $\zeta_{pn} = 0$.

$$A_{pn}^{(2)} = \frac{a}{2\pi}\int_0^{\infty} \rho Q(\rho)\, J_0^2(\rho a) \times I_{p+1}(\gamma_1 l)I_{n+1}(\gamma_1 l)e^{-2\gamma_1 l}/\gamma_1\, d\rho. \qquad (16)$$

The singularity of the core of the IDE is expressed in slow convergence of integral for ρ in expression (15).

The integral (15) has been solved numerically. The integral has been divided into four integrals with the following intervals of integrations $[0, k_1]$, $[k_1, C]$, $[C, E]$, $[E, \infty)$. Constants C, E are chosen under the assumption that $Cl \gg \max(p, n)$, $Ea \gg 1$. Performing the change of variables: for the first integral – $\rho = k_1\cos\psi$, for the second one – $\rho = k_1\mathrm{ch}\theta$. Both integrals are solved using a rectangular formula. Bessel functions are replaced with its asymptote $J_{p+1}(\gamma l)J_{n+1}(\gamma l) \approx (1/\pi\gamma l)cos\left((p - n/2)\pi\right)$ in the third integral. The modified integral is solved using a rectangular formula. Bessel functions are also replaced with their asymptote in the fourth integral. However, the modified integral is solved analytically. Thus, slow decreasing (as γ^{-2} if $\gamma \to \infty$) of integration element (15) is accounted. Integrals (16) are solved in the same way.

Let us analyze diffraction on the system of several CNT-dipoles. In this case, it is also not difficult to define the

https://doi.org/10.1017/S1759078713000196 Published online by Cambridge University Press

system of IDEs and to solve it using the Galerkin method. Matrix elements of the SLAE that defines interaction between dipoles are of the same form as (14). The difference is that the source point and the observation point are located on different CNT. In this case, GF does not have a singularity. That is why it is natural to use singular part of GF in the following form:

$$g_0(x, x', y, y', z, z') = \frac{e^{-ik_1 R}}{4\pi R},$$
$$R = \sqrt{(x-x')^2 + (y-y')^2 + (z-z')^2}, \qquad (17)$$

and to take integrals in (14) numerically over quadratures of a pinpoint accuracy. This has been done, for example, in [19, 20]. However, the distance between CNTs can be much smaller than its length. In this case, the order of the quadratures and calculating time grow dramatically. Therefore, we will detach the static part in (17) and use the following integral representation:

$$\frac{1}{R} = \frac{1}{\pi}\int_{-\infty}^{\infty} K_0(\gamma r) e^{i\gamma(z-z')} d\gamma,$$

$$g_0(x, x', y, y', z, z') = g_{01}(x, x', y, y', z, z') + g_{02}(x, x', y, y', z, z')$$
$$= \frac{1}{4\pi}\left[\frac{e^{-ik_1 R} - 1}{R} + \frac{1}{\pi}\int_{-\infty}^{\infty} K_0(\gamma r) e^{i\gamma(z-z')} d\gamma\right].$$

Now integrals with GF g_{01} can be easily solved numerically for all values of R and matrix elements with GF g_{02} are expressed using the Fourier integral. Conversions of these matrix elements including convergence acceleration of integrals are similar to the ones described above. Since it does not depend on frequency, it is enough to solve it once. This calculation method repeatedly decreases the calculation time.

IDE for nanodipoles lying on the substrate [5] (that is more complicated) is solved in the same way.

III. OPTICAL METALLIC ANTENNAS

We are using well-known three-dimensional IDE for the dielectric object [21] for modeling OA (Fig. 1):

$$\mathbf{E}(x, y, z) = \left[graddiv + k^2\right]\int_V \tau \mathbf{E}(x', y', z') g(R) dv' + \mathbf{E}^{ext}(x, y, z); \qquad (18)$$

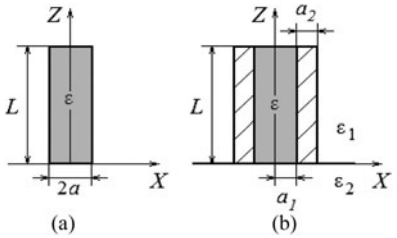

Fig. 1. Nanovibrators – OAs. (a) nanovibrator and (b) nanovibrator on the substrate ε_2, coated with the metal layer.

where $g(R)$ is the GF, $\tau = \varepsilon_s - \varepsilon$, ε_s is dielectric permittivity of the object, ε is the dielectric permittivity of the dielectric, surrounding the object, and k is the wave number inside it.

Values for complex dielectric constants of metals and refractive index of ZnO in optical range are presented in website [22]. These experimental results are well approximated by a formula for dielectric conductivity for plasma:

$$\varepsilon_s' = 1 - \left(\lambda/\lambda_p\right)^2,$$
$$\varepsilon_s'' = -\lambda^3 G/\left(2\pi c \lambda_p^2\right), \quad \varepsilon_s = \varepsilon_s' - i\varepsilon_s'',$$

where λ_p is the plasma wavelength, G is the collision frequency of electrons. For copper, $\lambda_p = 151.9$ nm, $G = -0.25 \times 10^{15}$ Hz, for silver $\lambda_p = 147$ nm and $G = -0.135 \times 10^{15}$ Hz [23].

Let us analyze the dielectric cylinder with radius a and length $2l$ lying along z-axis with the center placed in the origin of coordinates (picture 1). If $a \ll l$, we can consider that the electric field intensity has only one component parallel to Z-axis and depends only on coordinates r, Z. In this case, equation (18) can be modified to two-dimensional IDE:

$$\frac{j(r, z)}{\tau(r)} = E^{ext}(r, z) + \left[\frac{d^2}{dz^2} + k^2\right] \times \int_{-l}^{l}\int_{0}^{a} j(r', z') g(r, r', z, z') r dr' dz', \qquad (19)$$

where $j(r, z) = \tau(r)E(r, z)$ and GF for OA perpendicular to the substrate is of the form (6) and for OA without a substrate is of the form (7).

First, let us analyze OA without the substrate. The kernel of IDE (19) $G(r, r', z, z')$ has a logarithmic singularity. Presenting it in the form of Fourier integral in the same way as that for CNT:

$$g(R) = \frac{1}{4\pi^2}\int_{-\infty}^{\infty} K_0(\delta\kappa)\, e^{-i\rho(z-z')} d\rho,$$
$$\text{where } \kappa = \sqrt{r^2 + r'^2 - 2rr'\cos\phi},\ \delta = \sqrt{\rho^2 - k^2}.$$

Then

$$g(r, r', z, z') = \frac{1}{4\pi}\int_{-\infty}^{\infty} \tilde{g}(r, r', \gamma)\, e^{-i\gamma(z-z')} d\gamma, \qquad (20)$$

where

$$\tilde{g}(r, r', \gamma) = \begin{cases} I_0(r\delta)K_0(r'\delta), & r \le r', \\ I_0(r'\delta)K_0(r\delta), & r \ge r'. \end{cases} \qquad (21)$$

IDE (19) is solved using the Galerkin method. Resolving an unknown function $j(r, z)$ into weighted Chebyshev polynomials of the second order we obtain

$$j(r, z) = \sum_{m=0}^{\infty} Z_m(r)\, \bar{U}_m\left(\frac{z}{l}\right),$$
$$\bar{U}_m\left(\frac{z}{l}\right) = i^m \frac{1}{\pi l}\frac{1}{m+1}(l^2 - z^2)^{1/2} U_m\left(\frac{z}{l}\right). \qquad (22)$$

In (22), $Z_m(r)$ are unknown functions, in contrast with (12), where X_n are unknown coefficients.

https://doi.org/10.1017/S1759078713000196 Published online by Cambridge University Press

Let us substitute (22) into (19) and project on $\bar{U}_n(z/l)$. As a result we will obtain the following system of IEs

$$\sum_{m=0}^{\infty}\frac{Z_m(r)D_{nm}}{\tau(r)} = B_n(r) + \frac{1}{2\pi}\sum_{m=0}^{\infty}\int_{-\infty}^{\infty}(\gamma^2-k^2)\frac{J_{m+1}(\gamma l)}{\gamma}\frac{J_{n+1}(\gamma l)}{\gamma}d\gamma \times\int_0^{\infty} r'\,Z_m(r')\tilde{g}(r,r',\gamma)dr',\ m=0,1,2\ldots \quad (23)$$

where

$$D_{nm}=\int_{-l}^{l}\bar{U}_n\left(\frac{z}{l}\right)\bar{U}_m\left(\frac{z}{l}\right)dz = \begin{cases} 0, & m \text{ and } n \text{ of the different parity} \\ \frac{l}{\pi^2}\cos\left(q\frac{\pi}{2}\right)\frac{1}{m}\frac{1}{n}\left[\frac{1}{p^2-1}-\frac{1}{q^2-1}\right], & m \text{ and } n \text{ of the same parity,} \\ & q=m-n,\ p=m+n \end{cases}$$

$$B_n(r)=\frac{1}{2\pi}\int_0^{2\pi}d\phi\int_{-l}^{l}\bar{U}_m\left(\frac{z}{l}\right)E^{ext}(r,z)dz = E_0\sin\theta J_0(k_{-|-}r_q)\frac{J_{n+1}(k_z l)}{k_z},\ k_{-|-}^2=k_x^2+k_y^2,$$

IE (23) are solved by the collocation method. We use quadrature $\int_0^a r'f(r')dr'=\sum_{p=1}^{P}\bar{A}_p f(r_p)$ and require the fulfillment of (23) in quadrature nodes. We use the notations $\bar{A}_p Z_m(r_p)=X_{mp}$ – unknown coefficients, $B_{nq}=B_n(r_q)$. In (23), we are taking into consideration only first M equations. As a result, we obtain the SLAE:

$$\sum_{m=0}^{M}X_{mp}\frac{D_{nm}}{\bar{A}_q\tau(r_q)}=B_{nq}+\sum_{m=0}^{M}\sum_{p=1}^{P}X_{mp}A_{nm}^{qp},\quad n=0,1,\ldots M,\ q=1,\ldots,P, \quad (24)$$

where

$$A_{nm}^{qp}=\begin{cases}\frac{1}{\pi}\int_0^{\infty}(\gamma^2-k^2)\frac{J_m(\gamma l)}{\gamma} \times\frac{J_n(\gamma l)}{\gamma}\tilde{g}(r_p,r_q,\gamma)d\gamma, & m \text{ and } n \text{ of the same parity,} \\ 0, & m \text{ and } n \text{ of the different parity.}\end{cases} \quad (25)$$

Using integral representation of singular core (20) helps us to overcome difficulties associated with solving integrals of bisingular functions in the same way as that in the previous case. In this case, the singularity of the core of IDE is expressed in slow convergence of integrals in spectral space (25). It is easier to improve convergence of integrals using the method described above than to perform regularization.

After solving the final SLAE (24), we derive an unknown function $j(r,z)$.

It is not difficult to derive an expression for the far field:

$$E_\vartheta = H_\phi Z_0 \approx \frac{e^{-ikr}}{4\pi(r/l)}F(\vartheta),$$

where

$$F(\vartheta)=\frac{2\pi k^2}{l}\int_0^a r'\tau(r')J_0(r'\sin\vartheta)dr' \times\int_{-l}^{l}j(r',z')e^{ik\cos\vartheta z'}dz',$$

where ϑ is the observation angle, counted from dipole, $F(\vartheta)$ is the non-dimensional scattering diagram.

Solution of IDE (19) is similar for OA on the substrate. The singular part of GF is located in the first term that is GF for the task resolved above.

The derived solution can be easily generalized on the diffraction on several dielectric cylinders.

IV. PLANAR METAL OAS

Here, we investigate the OA system consisting of a system of N rectangular dipoles deposited on the dielectric substrate.

We use the Cartesian coordinate system where plane $y=0$ corresponds to the top of the substrate. Dipoles are parallel to the z-axis and perpendicular to the x-axis. Permittivity of substrate is denoted by ε_2, and permittivity of dielectric is $\varepsilon_1=1$. Let us consider scattering of the plane wave. At first, we consider one dipole with length $2l$ 2a, $a\ll l$. It is supposed that the surface current on dipoles has a longitudinal component j_z only.

Avoiding calculation of the field within metal film is possible by using the method of ABC for the dielectric layer [24]. We suppose that ABC is valid on metal surface:

$$E_z=-i\tau j_z, \quad (26)$$

where $\tau=Z_0/k\delta,\ \delta=(\varepsilon_s-\varepsilon_1)t$, Z_0, k are wave resistance and wave number in free space, ε_s, t are permittivity and width of dipoles.

Let us introduce the term "external electromagnetic field" $\vec{E}^{ext}$. This term means the sum of field of incident wave and transmitted and reflected from substrate without strips.

Applying two-dimensional Fourier transform, we can obtain expressions for components of the electromagnetic field:

$$E_x(x,y,z)=\frac{iZ_0}{4\pi^2 k}\int_{-\infty}^{\infty}\int_{-\infty}^{\infty}\alpha\gamma U_e(\rho)\tilde{j}_z(\alpha,\gamma) \times\exp\left[i(\alpha x+\gamma z)\right]V_1(\rho,y)d\alpha d\gamma,$$
$$E_y(x,y,z)=\frac{Z_0}{4\pi^2 k}\int_{-\infty}^{\infty}\int_{-\infty}^{\infty}\gamma U_e(\rho)\tilde{j}_z(\alpha,\gamma) \times\exp\left[i(\alpha x+\gamma z)\right]V_2(\rho,y)d\alpha d\gamma,$$
$$E_z(x,y,z)=\frac{iZ_0}{4\pi^2 k}\int_{-\infty}^{\infty}\int_{-\infty}^{\infty}[\gamma^2 U_e-k^2U_m]\tilde{j}_z(\alpha,\gamma) \times\exp\left[i(\alpha x+\gamma z)\right]V_1(\rho,y)d\alpha d\gamma, \quad (27)$$

https://doi.org/10.1017/S1759078713000196 Published online by Cambridge University Press

where

$$U_e(\rho) = \frac{1}{\varepsilon_1\beta_2 + \varepsilon_2\beta_1},\ U_m(\rho) = \frac{1}{\beta_1 + \beta_2},$$
$$\beta_{1,2} = \sqrt{\rho^2 - k^2\varepsilon_{1,2}},\ \rho = \sqrt{\alpha^2 + \beta^2},$$

$\tilde{j}_z(\alpha, \gamma)$ is the two-dimensional Fourier transform of $j_z(x, z)$,

$$V_1(\rho, y) = \begin{cases} \exp(-\beta_1 y),\ y \geq 0, \\ \exp(\beta_2 y),\ y \leq 0, \end{cases}$$

$$V_2(\rho, y) = \begin{cases} -\beta_2 \exp(-\beta_1 y),\ y \geq 0, \\ \beta_1 \exp(\beta_2 y),\ y \leq 0. \end{cases}$$

After substitution of (27) in ABC (26) we have

$$-\frac{iZ_0}{k}\left[\frac{d^2}{dz^2}\int_{-l}^{l}\int_{-a}^{a} j(x', z')g_e(x, x', z, z')dx'dz' + k^2\int_{-l}^{l}\int_{-a}^{a} j(x', z')g_m(x, x', z, z')dx''dz'\right] + E_z^{ext}(x, z) = -i\tau j_z(x, z),\ |x| \leq a,\ |z| \leq l, \quad (28)$$

where $g_{e,m}(x, x', z, z') = \frac{1}{4\pi^2}\int_{-\infty}^{\infty}\int_{-\infty}^{\infty} U_{e,m}(\rho)\exp[i(\alpha\bar{x} + \gamma\bar{z})]$ $d\alpha d\gamma$, $\bar{x} = x - x'$, $\bar{z} = z - z'$. Let us present an unknown function $j_z(x, z)$ in the following form:

$$j_z(x, z) = I(z)/(\pi\sqrt{a^2 - x^2}), \quad (29)$$

where $I(z)$ is the current on strip. The singularity at the edge of the strips of the form $1/\sqrt{a^2 - x^2}$ is typical for ideal conducting metal. For the impedance strip, the current rises at the edges. Numerical results [16] show that the singularity in the form of $1/\sqrt{a^2 - x^2}$ has good internal convergence of solution for impedance strips as well. This singularity makes it possible to simplify analytical transformation of the Fourier integrals.

Let us substitute (29) into IDE (28), which requires the fulfillment of IDE at $x = 0$. As a result, we have

$$-\frac{iZ_0}{k}\left[\frac{d^2}{dz^2}\int_{-l}^{l} I(z')\hat{g}_e(z, z')dz' + k^2\int_{-l}^{l} I(z')g_m(z, z')dz'\right] + E_z^{ext}(0, z) = -i\tau I_z(z)/(\pi a),\ |z| \leq l, \quad (30)$$

where

$$\hat{g}_{e,m}(z, z') = \frac{1}{4\pi^2}\int_{-\infty}^{\infty}\int_{-\infty}^{\infty} U_{e,m}(\rho)J_0(\alpha a) \times \exp(i\gamma\bar{z})d\alpha d\gamma.$$

To solve IDE (30), we use Galerkin's method with basis functions in the form of (13). As a result, we have SLAE. The calculation of matrix elements of the obtained system is similar to the previous case. It is possible to obtain a system of paired IEs for a system of dipoles. To solve this system, the method of Galerkin is also used.

To calculate the scattering diagram, the asymptotic [6] was applied to field components and expressed in the form of Fourier integral (27):

$$\frac{1}{4\pi^2}\int_{-\infty}^{\infty}\int_{-\infty}^{\infty} f(\alpha, \gamma)\frac{\exp(-\beta_1 y)}{\beta_1}\exp[i(\alpha x + \gamma z)]d\alpha d\gamma \approx f(\alpha_a, \gamma_a)\frac{\exp(-ik\sqrt{\varepsilon_1}r)}{2\pi r},$$

where $\alpha_a = -k\sqrt{\varepsilon_1}\sin\theta\cos\phi$, $\gamma_a = -k\sqrt{\varepsilon_1}\cos\theta$, r, θ, ϕ are spherical coordinates, angle θ counts from dipole, and angle ϕ counts from substrate. Components of the field in spherical coordinate system:

$$E_{\theta,\phi}(r, \theta, \phi) = F_{\theta,\phi}(\theta, \phi)\frac{\exp(-ik\sqrt{\varepsilon_1}r)}{4\pi r/l}.$$

V. NUMERICAL RESULTS

The algorithms presented here were implemented in C ++ program. As shown, kernels of integrals are the same for all the matrix elements. That is why these kernels can be evaluated only once along with values for $\tilde{V}_n(\gamma)$. Such an approach reduces the calculation time by an order of magnitude. For example, the time of calculation of one point of frequency characteristic is 0.4 s for CNT under substrate and 0.015 s for CNT in free space on PC with CPU 2.33 GHz. The time of calculation using the obtained method is 10 times less than in the case of using the modified collocation method [25, 26].

The analysis of internal convergence shows that the required number of basis functions (order of SLAE) increases, while the electrical length of nanodipoles and ε_1, ε_2 increases. For calculating the impedance Z_{in} with error $<1\%$ at frequency $f =$ 250 GHz (half of plasma wavelength fits along the dipole) it will be sufficient to take $M = 10$, at frequency $f = 1000$ GHz (eight half-wavelength fits along the dipole) – $M = 50$. Internal convergence of solution for the far-field is 3–5 times faster than for calculation of Z_{in} for any method of excitation.

For planar OA to achieve the same accuracy, it is sufficient to take 3–7 basis functions, and 3–7 basis functions for the cylindrical OA for each coordinate. Such precision, of course, is purely of theoretical interest, since it is much higher than the accuracy of the mathematical model.

Investigation of impedance Z_{in} of single-layer CNT-dipoles is carried out. In the figures the complex input resistance, normalized to the value $R_0 = (h/2e^2) \approx 12.9$ kΩ, is presented. For all figures, where the dimensions are not specified, it is supposed that $2l = 20$ μm, $a = 2.712$ nm.

The investigation of input impedance Z_{in} of isolated single-layer CNT-dipoles of various lengths is also presented (Fig. 2). Solid lines designate the real part of Z_{in}, dashed lines designate the imaginary part of Z_{in}.

In millimeter and submillimeter wavelength ranges, there are resonances at the frequency response at lengths of dipoles much smaller than the wavelength in free space. In the frequency range up to 1 THz, the nanotube, whose half-length $l = 10$ μm, has three distinct resonances. In a perfectly conducting dipole of the same length, the first resonance (first root of $Z_{in}(f) = 0$) is observed at a frequency of about 7.5 GHz. This effect is explained by the possibility of

https://doi.org/10.1017/S1759078713000196 Published online by Cambridge University Press

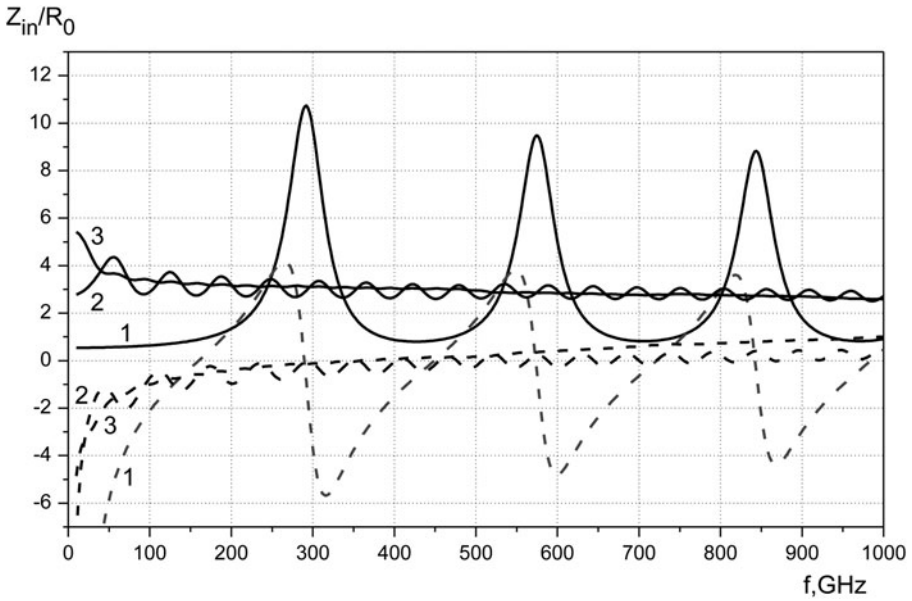

Fig. 2. Impedance of CNT-dipoles with different lengths. Curves 1 – $l = 10$ μm; 2 – $l = 50$ μm; 3 – $l = 100$ μm.

propagation of surface waves (plasmons) along the nanotube [1]. In the case of nanotube of length 50 μm, the number of resonances is much larger, and their amplitudes are less than the CNT's length (10 μm). It should be pointed out that the imaginary part of the input impedance of CNT with a length of 50 μm for frequency up to 300 GHz is negative. Thus, there are no resonances of radiation for the CNT with a length of 50 μm for frequencies up to 300 GHz. The average value of the real and imaginary parts of the input resistance of CNT with a length of 100 μm is of the same order with the case of nanotubes with 50 nm length, but without resonances. The nature of the input impedance of CNT with length of 100 μm is similar to the input resistance of the traditional dipole antenna, made of classical metal. Thus, with the increase of the length of the nanodipole the number of resonances increases, but the efficiency of the radiation decreases. Antenna parameters of CNT-dipole converge to the parameters of conventional electric dipole, perhaps surpassing them on Q-factor. As has been noted, the electrical length of the nanodipole is greater than the length of conventional electric dipole. Therefore, the current distribution on it is much more complex and there are several extremes (Fig. 3).

In Fig. 4 results of the frequency dependence of the radiation pattern for a system of 1, 3, and 5 nanodipoles are presented for observation angle $\theta = 90^\circ$ (normal to the dipole). In this case, the radiating nanotube is situated in the center of the system and the other nanotubes are receivers. The distance between the nanotubes is $d = 10$ nm.

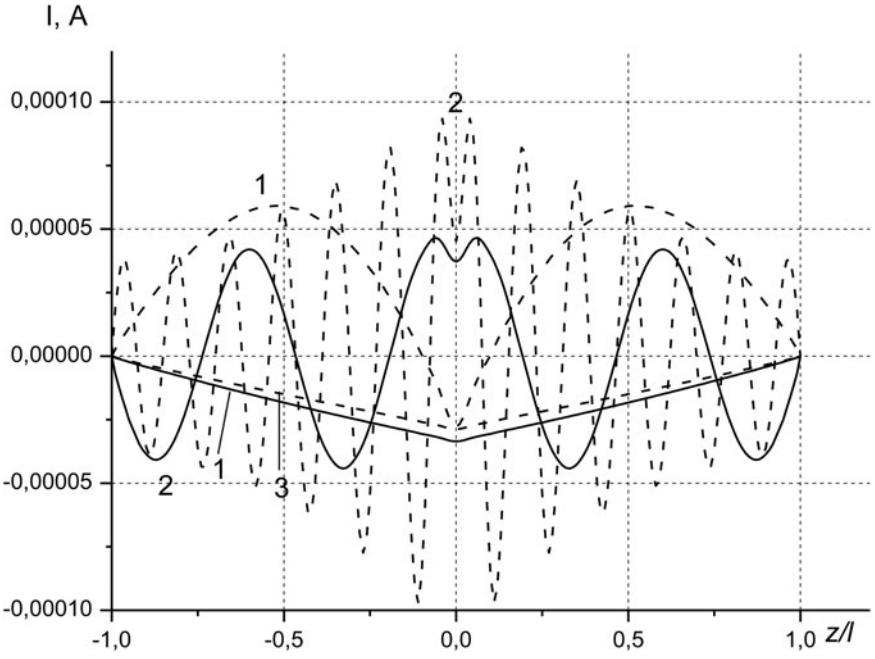

Fig. 3. Current distribution on nanodipole. Solid curves – $\varepsilon = 1$, dash curves – $\varepsilon = 10$. Curves: 1, $f = 100$ GHz; 2, $f = 1000$ GHz; 3, $f = 1000$ GHz, ideal metal.

https://doi.org/10.1017/S1759078713000196 Published online by Cambridge University Press

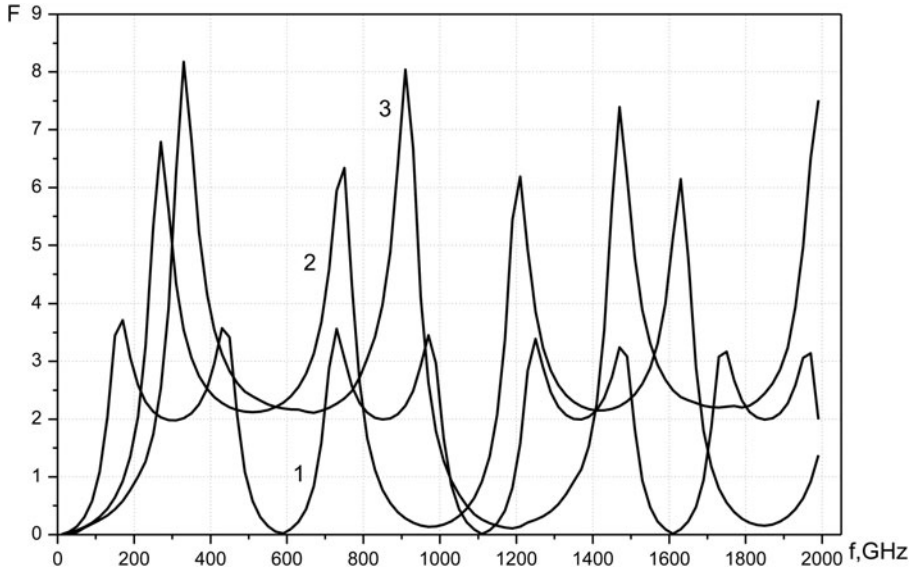

Fig. 4. Frequency response of far-field for problem of excitation of system of parallel nanodipoles. Curve 1 single nanotube; curve 2–3 nanotubes; curve 3–5 nanotubes.

The curves have extremes at the points where the imaginary part of the input impedance becomes zero (Fig. 2). In this case, the maximums (minimums) of function F correspond to the minimums (maximums) of the real part of input impedance. Maximum amplitude of far-field of system of three dipoles is two times higher than far-field magnitude of single dipole. Further increasing of the number of dipoles gives a significant increase of far-field amplitude also.

In Fig. 5 results of calculation of scattering pattern for the problem of plane wave diffraction are presented. The frequency dependencies of scattering pattern are shown at two values of observation angle. Maximums of radiation and scattering diagram are the same. Maximum level of scattering pattern decreases with increase of the frequency.

The form of scattering pattern and radiation pattern of dipole with $l \ll \lambda$ is weakly dependent on frequency.

Even for the second resonant frequency, there is only one lobe of scattering pattern. This is because the resonances of the amplitude–frequency characteristics of the scattered field and the current distribution $j(z)$ on a dipole are determined by the ratio of the dipole's length and length of a plasma wave in the CNT.

The form of scattering pattern and number of scattering lobes are determined mainly by the ratio of the dipole's length and the wavelength in free space λ:

$$F = const\ \cos\theta \int_{-l}^{l} j(z)\exp(ikz)dz.$$

For CNT-dipole at $f = 1500$ GHz, we have $l/\lambda = 0.05$.

To make the linear system of dipoles to have directivity in the H-plane, such as for traditional vibrators, the distance between the dipoles should be about one-quarter of the wavelength in free space. Thus, it is impossible to create a directional antenna array of CNTs which have nanoscale sizes.

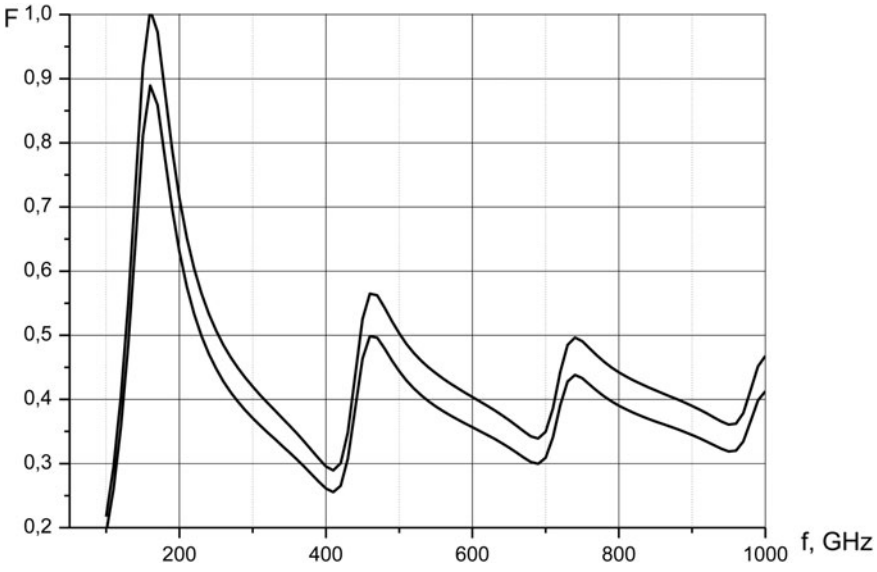

Fig. 5. Frequency response of far-field for diffraction problem. Incidence angle is equal to observation angle –90° (upper curve), 70° (bottom curve).

https://doi.org/10.1017/S1759078713000196 Published online by Cambridge University Press

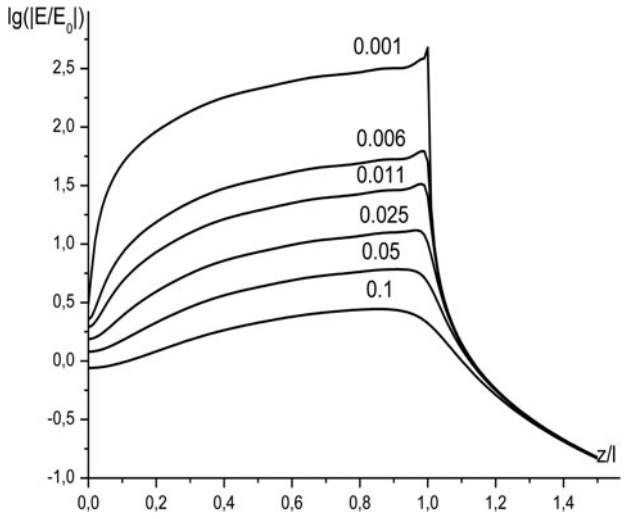

Fig. 6. Normalized intensity of electric field near dipole. Caption near the curves denotes normalized to $l = L/2$ distance to nanodipole.

Results of calculation of near field of CNT without the substrate are presented in Fig. 6. The origin of the coordinate is at the center of CNT. Owing to the symmetry of the problem, the field is shown for $z > o$ case only. The amplitude of the field near the CNT is 2–3 orders of magnitude higher than the external field. The intensity of the field rapidly decreases with the increase of distance from CNT.

Now let us consider the frequency response of OA. The dependence of the scattered field on the wavelength has a resonant character (Figs 7 and 8). There are two resonances at the defined size and type of excitation. At the first resonance, one half-wavelength fits along the dipole, at the second, three half-wavelengths. The amplitude of the first resonance is much higher than the amplitude of the second resonance. The resonant wavelength of the CNT-dipole is greater than the resonant wavelengths of the perfectly conducting dipole of the same size. Of course, the resonant wavelength increases when the length of the dipole increases. For a given length of CNT-dipole λ_r can be changed in a wide range by changing the type of metal and its thickness. The intensity of the scattered field of CNT-dipole increases with the increase of the radius, but it is smaller than that of a perfectly conducting dipole. It should be noted that there is a dependence of λ_r on the radius and thickness of the metal coating. For dielectric and an ideal metal dipole λ_r increases with the radius a, and for the metal dipole, the dependence is inverse (Fig. 7).

In the case of diffraction on a metal film coated with nanocrystal ZnO (Fig. 8), the resonance is observed even when the film thickness t is of a few nanometers. The resonant wavelength is strongly dependent on the thickness of the coating. For comparison, the figure also shows the characteristics of fully metal dipoles. It is shown that at $t = 20$ nm (curve 4), the characteristics of the nanocrystal and copper dipole (curve 6) are close. For smaller t, the field penetrates into the nanocrystal, thus increasing its influence on the scattering diagram.

The above-mentioned dependence of λ_r on the radius and thickness of the metal coating can be explained by a simple formula for estimating the resonance wavelength mth resonance:

$$\lambda_r^{(m)} = \frac{c}{\nu}\frac{2L_e}{m},$$

where c is the speed of light in free space, ν is the propagation speed of wave along dipole, and L_e is the electric (effective) length of dipole, $L_e > L$, L_e depends on L/a and the frequency.

For the ideal dipole, it is valid that $\nu = c$ and the dependence $\lambda_r^{(m)}(a)$ is explained by the dependence $L_e(a)$. For a dielectric or non-ideal conducting metal dipole, the dependence $\lambda_r^{(m)}(a)$ is explained by the dependence of moderating ratio $n = c/\nu$ on radius. If the wave propagates along the dielectric cylinder, then the field is concentrated within the dielectric and exponentially decreases outside the dielectric.

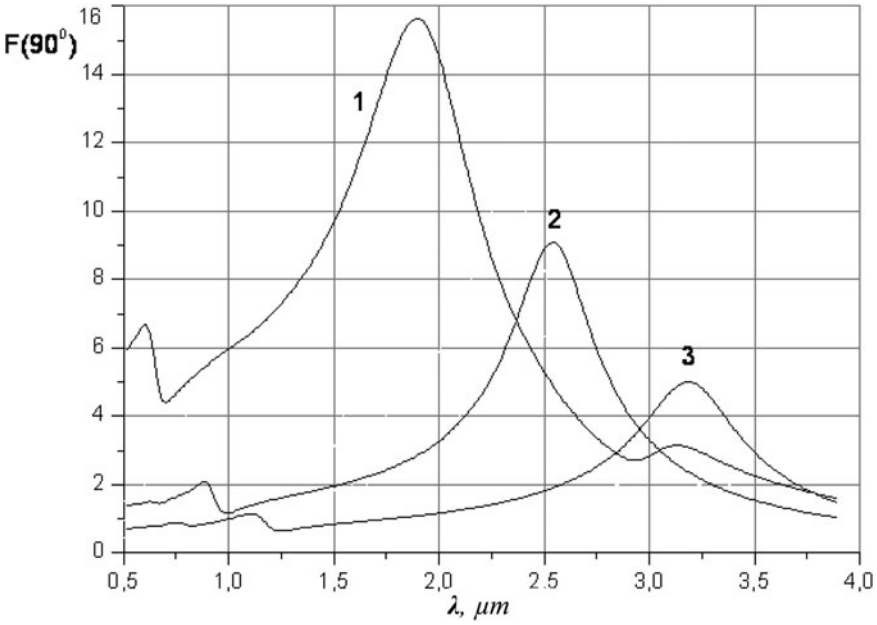

Fig. 7. Characteristics of copper nanodipoles with different radius; $L = 0.7$ μm. Curves 1–3 denote different radii a (μm): 0.02, 0.015, and 0.01.

https://doi.org/10.1017/S1759078713000196 Published online by Cambridge University Press

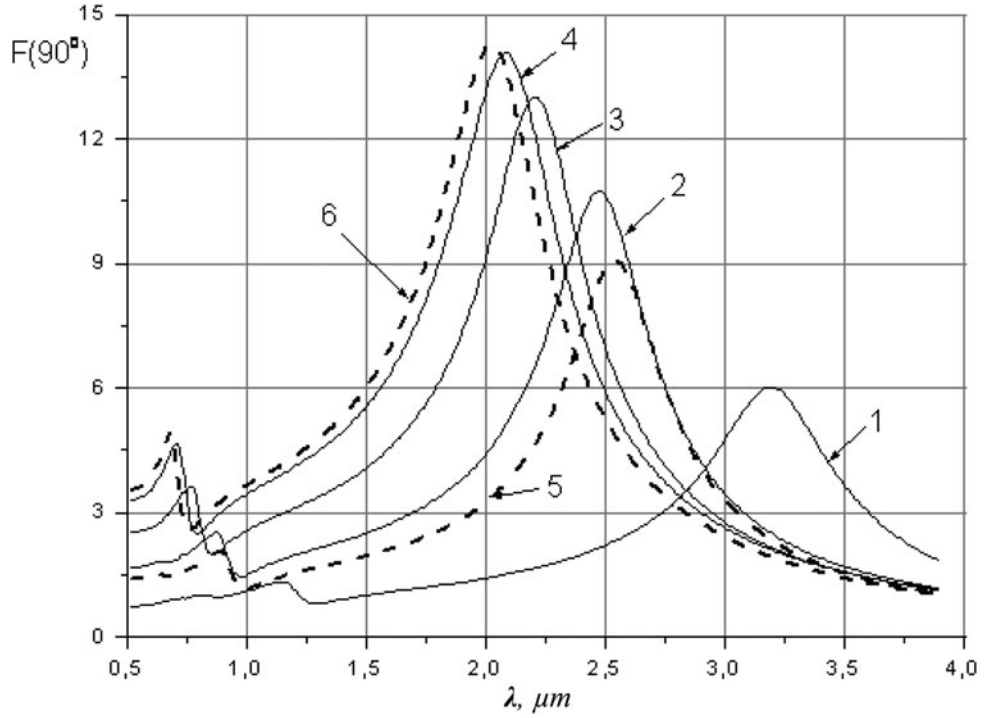

Fig. 8. Characteristics of nanodipole from ZnO (radius 0.01 μm, $L = 0.7$ μm) with different thickness of copper layer. Curves 1–4 correspond to thickness of coating: 5, 10, 15, and 20 nm. Curves 5 and 6, copper nanodipole with radii of 15 and 30 nm.

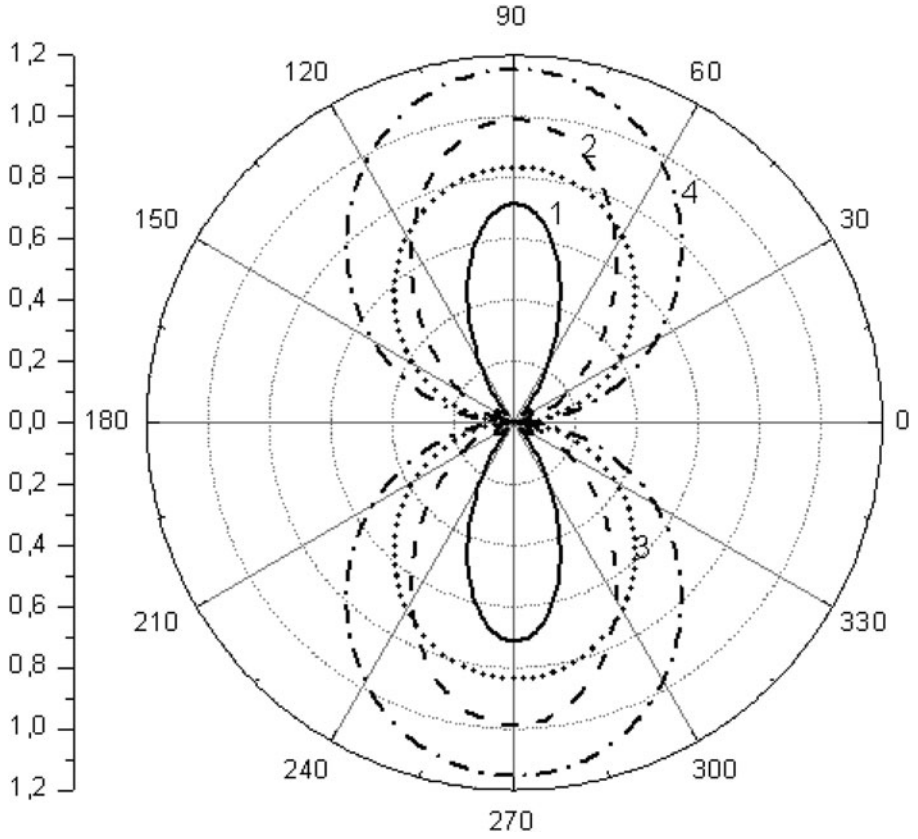

Fig. 9. Scattering diagram of copper nanodipole with normal incidence, $L = 0.7$ μm, $a = 0.01$ μm. Curves 1–4 denote λ (μm): 0.5, 1.0, 1.5, and 2.0.

https://doi.org/10.1017/S1759078713000196 Published online by Cambridge University Press

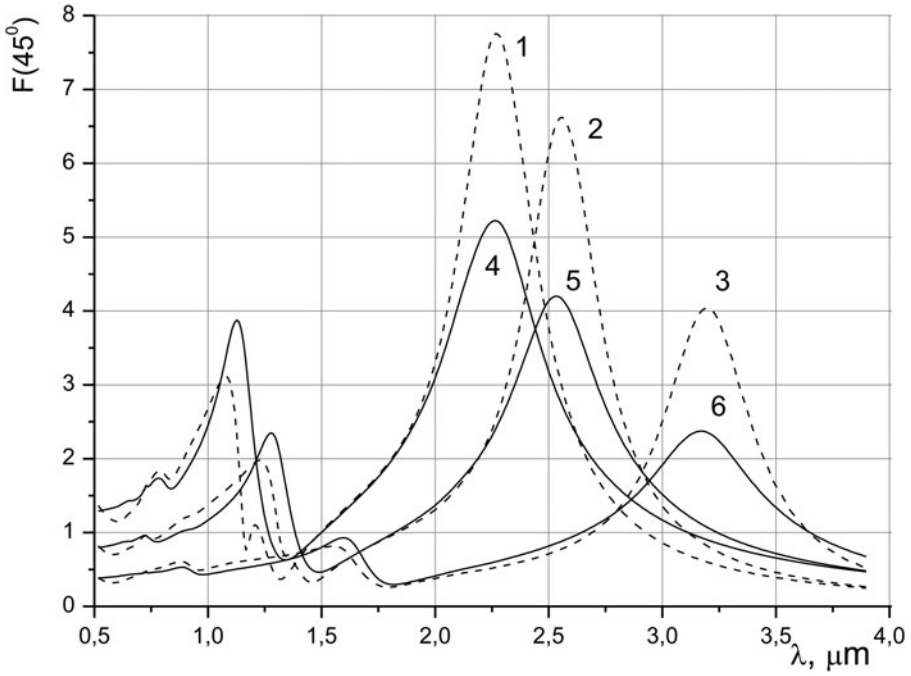

Fig. 10. Frequency response of copper nanodipole on substrate with $\varepsilon = 4.11$ (curves 1–3) and without substrate (curves 4–6), $L = 0.7$ μm, curves 1, 4 – $a =$ 0.02 μm, curves 2, 5 –$a = 0.015$ μm, curves 3, 6 – $a = 0.01$ μm.

If the radius increases the moderating ratio increases, as a result of this $\lambda_r^{(m)}$ increases too.

At the interface between the dielectric (in our case the free space) and the plasma (electron plasma of metal), the field of the surface wave (plasmon) exponentially decays with increase of the distance from the border in both directions (dielectric and metal). When reducing the thickness of the metal, the interaction of plasmons, propagating on the opposite sides of the metal, increases. In this case, the moderating ratio n and, therefore, $\lambda_r^{(m)}$, increase with the decrease of the radius. This relationship $n(a)$ is easily obtained from the analysis of dispersion equation for the E-wave propagating in the plasma layer [17].

The field distribution near the OA is similar to the field near the CNT (Fig. 6). Near the OA, the field is 2–3 orders of magnitude higher than the external field. The field strength decays rapidly with the distance from the OA.

The scattering diagram of metal nanodipoles (Fig. 9) is close to the scattering diagram of perfectly conducting dipoles with greater length.

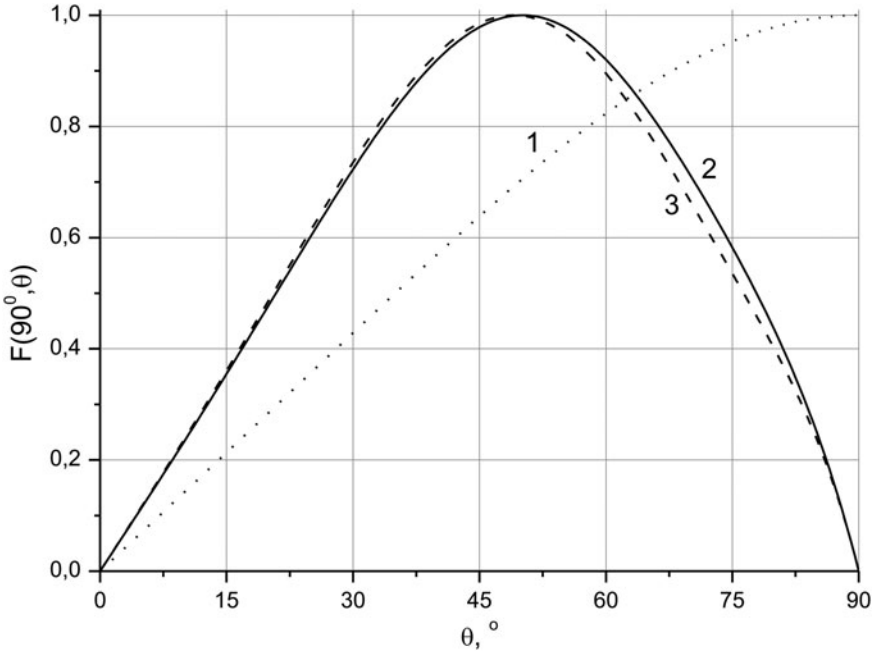

Fig. 11. Normalized scattering diagram of copper nanodipole on the substrate, $\lambda = 1$ μm, $L = 0.7$ μm, a = 0.02 μm, permittivity of substrate defined by curves: 1, $\varepsilon = 1$; 2, $\varepsilon = 4$; 3, $\varepsilon = 10$.

https://doi.org/10.1017/S1759078713000196 Published online by Cambridge University Press

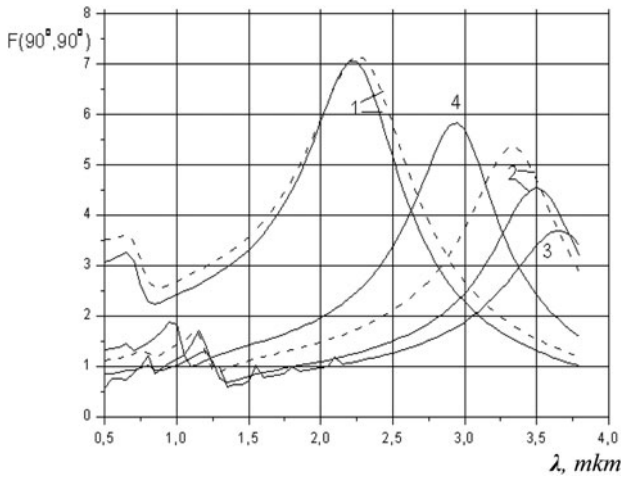

Fig. 12. Comparison of characteristics of planar metal nanodipole; $l = 0.35$ μm, solid curves denote $a = 0.025$ μm, dash curves $a = 0.035$ μm. Curves: 1, ideal conducting dipole; 2, copper nanodipole, $t = 0.01$ μm; 3, gold nanodipole, $t = 0.01$ μm; 4, copper nanodipole, $t = 0.02$ μm.

Resonant wavelengths of nanodipoles on the substrate are almost independent of its dielectric constant, the main difference is the change in emission intensity (Fig. 10). The results are presented for angle of incidence $\theta = 45^{\circ}$. The presence of the substrate leads to a fundamental change in the form of the scattering diagram (Fig. 11).

Characteristics of planar metal OA (Fig. 12) are qualitatively similar to that of the cylindrical OA.

Figure 13 shows the characteristics of antennas, consisting of several parallel nanodipoles. For comparison, the curve for a single dipole is also shown. The distance between the nanodipole $d = 0.1$ μm is close to $\lambda/\left(4\sqrt{(\varepsilon_1 + \varepsilon_2)/(2)}\right)$ at $\lambda = 0.8$ μm. Therefore, at the increase of number of nanodipoles, the amplitude of the scattered field at the short-wavelength resonance becomes comparable and further exceeds the amplitude of the long-wavelength resonance.

Maximum of scattering diagram (Fig. 14) comes nearer to the direction of specular scattering.

VI. CONCLUSIONS

(1) Original mathematical methods, algorithms and programs on C ++ programming language were developed for theoretical study of radiophysical properties of nanodipoles.
   (a) The solution of the problem of excitation of CNT-nanodipoles on dielectric substrate was reduced for solving PIEs. The use of PIEs is more preferable than IDEs because GF of the problem is expressed in Fourier integral. By means of the Galerkin method with Chebyshev basis, the solution of PIEs was reduced to the solution of SLAE, where matrix elements are also expressed in the Fourier integrals. Such an expression of the kernel and matrix elements allows us to easily overcome difficulties, related to kernels' singularity. The singularity of the kernel of IDEs, while solving PIEs appears in slow convergence of integrals in matrix elements of the SLAE. The convergence of these integrals was enhanced. Rapid internal convergence of the solution has been shown. The software, based on the solution of PIEs, allows us to calculate faster than the software, based on the modified collocation method [25–27].
   (b) The solution of the boundary problem of optical frequency electromagnetic waves diffraction on the metallo-dielectric dipoles–nanocrystals was reduced to a solution of IDEs for inhomogeneous dielectric cylinder. Kernels of equations were expressed in the form of Fourier integral. IDEs were solved by combining the Galerkin and the collocation methods.

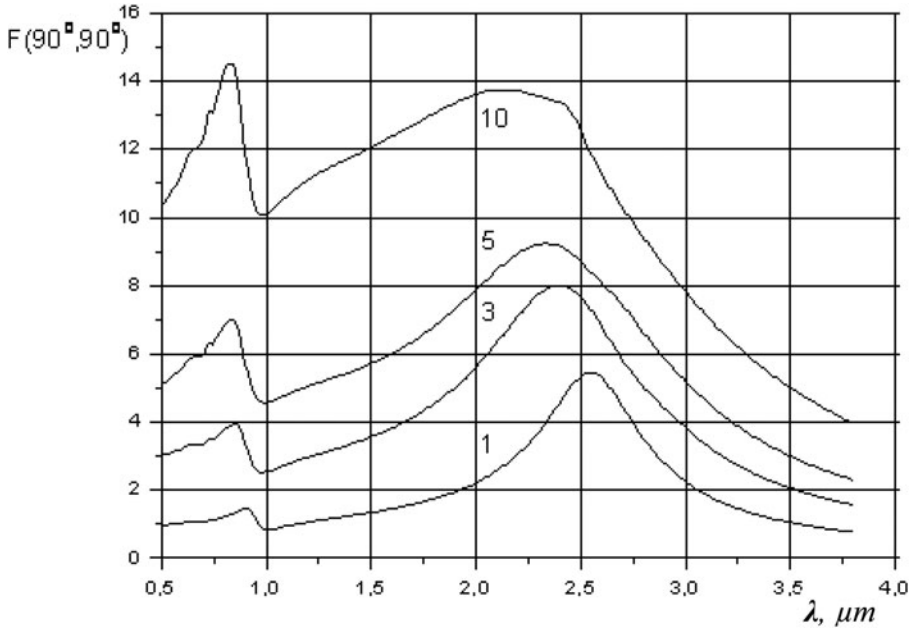

Fig. 13. Characteristics of system of metal nanodipoles. Captions near the curves designate the number of nanodipoles in the system N, $a = 0.03$ μm, $t = 0.01$ μm, $l = 0.25$ μm, $d = 0.1$ μm.

https://doi.org/10.1017/S1759078713000196 Published online by Cambridge University Press

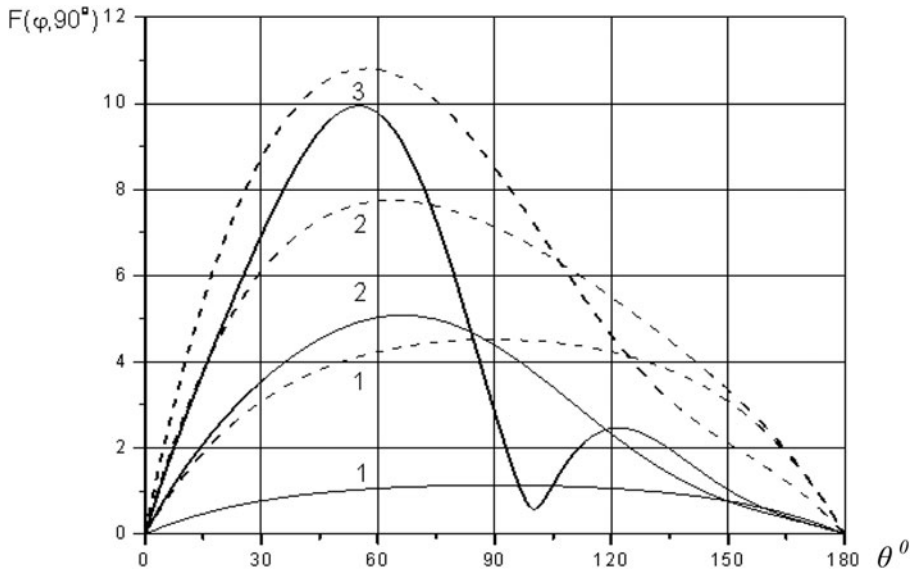

Fig. 14. Scattering pattern of system of metal nanodipoles; $l = 0.25$ μm, $a = 0.03$ μm, $t = 0.01$ μm, $d = 0.1$ μm. Wave is polarized along nanodipole, incidence angle −45°. Solid curves: λ_r =0.85 μm; dash curves: $\lambda_r = 2.5$ μm. Curves: 1, single nanodipole; 2–5, nanodipoles; 3–10, nanodipoles.

(c) By means of the method of ABCs for the thin dielectric layer (taking into account the finite value of metals' permittivity in the optical range), the solution of the boundary problem of diffraction on metallic nanodipole was reduced to the solution of PIEs. PIEs were solved by the collocation method. The matrix elements of obtained SLAE are expressed in the form of the Fourier integrals. To verify results and estimate the accuracy, the IE for dielectric elliptical cylinder of finite length was obtained and solved by means of the method, combining the Galerkin and the collocation method.

(2) The results of investigation of CNT-nanodipoles in millimeter and submillimeter wavelength ranges.

(a) In millimeter and submillimeter wavelength range, there are resonances on amplitude–frequency characteristic at dipole length much less than wavelength in a vacuum. An increase of nanoantenna's length leads to an increase in the number of resonances in the frequency range under investigation and to an efficiency drop. CNT-nanoantenna's parameters come nearer to the parameters of conventional metallic dipole. Thus, simple increase of nanotube's length does not allow us to obtain efficient radiation in centimeter wavelength range.

(b) The influence of substrate on amplitude–frequency characteristics of CNT-nanoantenna was investigated. It was shown that these characteristics could be described by the introduction of effective dielectric permittivity $\varepsilon_{ef} = (\varepsilon_1 + \varepsilon_2)/2$ only at low frequencies and low values of substrate's dielectric constant. The distinctions between radiation pattern of nanodipoles over the substrate and isolated nanodipoles have been mentioned.

(c) The properties of finite grating of the nanodipoles have been investigated. Getting the CNTs closer leads to an increase in resonant frequency and amplitude of the diffracted field. The dependence of amplitude on the number of nanodipoles is nonlinear. It was shown that in centimeter and millimeter frequency ranges it is impossible to create the grating of CNTs, which has nanoscale sizes.

(d) The investigations of the frequency-selective surface based on the doubly periodic grating of CNT–nanodipoles have shown the possibility of obtaining high values of the reflection coefficient.

(3) The properties of metallic nanodipoles and nanocrystals–dipoles coated with metallic film were theoretically investigated.

(a) The dependence of scattered field on the frequency has a resonant character. Resonant wavelengths of nanodipoles are greater than resonant wavelength for perfectly conducting dipole of the same dimension. The resonances are observed even if the thickness of the metallic film, coating the nanocrystal, is about 3–5 nm.

(b) The possibility of creation of directional OA, consisting of grating of planar nanodipoles, has been shown.

REFERENCES

[1] Diachkov, P.N.: Elektronnye svoistva i primenenie nanotrubok. BINOM. Laboratoria Znaniy, Moscow, 2010.

[2] Slepyan, G.Ya.; Maksimenko, S.A.; Lakhtakia, A.; Yevtushenko, O.M.; Gusakov, A.V.: Electrodynamics of carbon nanotubes: dynamic conductivity, impedance boundary conditions and surface wave propagation. Phys. Rev. B, **60** (1999), 17136–17149.

[3] Hanson, G.W.: Fundamental transmitting properties of carbon nanotube antennas. IEEE Trans. Antennas Propag., **53** (11) (2005), 3426–3435.

[4] Slepyan, G.Ya.; Shuba, M.V.; Maksimenko, S.A.; Lakhtakia, A.: Theory of optical scattering by achiral carbon nanotubes, and their potential as optical nanoantennas. Phys. Rev. B, **73** (2006), 195416.

[5] Lerer, A.M.: The radio-transmitting properties of a carbon nanotube vibrator located on the boundary of a dielectric. Moscow Univ. Phys. Bull., **65** (5) (2010), 378–385.

[6] Lerer, A.M.; Sinyavsky, G.P.: Diffraction of an electromagnetic wave on the finite lattice. Moscow Univ. Phys. Bull., **65** (6) (2010), 476–481.

[7] Bharadwaj, P.; Deutsch, B.; Novotny, L.: Optical antennas. Adv. Opt. Photon., **1** (2009), 438.

[8] Klimov, V.V.: Nanoplazmonika. Phizmatlit, Moscow, 2010, 480p.

[9] Klimov, V.V.: Nanoplazmonika. Usp. Fiz. Nauk., **178** (8) (2008), 875.

https://doi.org/10.1017/S1759078713000196 Published online by Cambridge University Press

[10] Kempa, K. et al.: Carbon nanotubes as optical antennae. Adv. Mater, **19** (2007), 421.

[11] Salandrino, A.; Li, J.; Engheta, N.: Shaping light beams in the nanometer scale: a Yagi-Uda nanoantenna in the optical domain. Phys. Rev. B., **76** (2007), 245403.

[12] Huang, J.S.; Feichtner, T.; Biagioni, P.; Hecht, B.: Impedance matching and emission properties of nanoantennas in an optical nanocircuit. Nano Lett., **9** (5) (2009), 1897.

[13] Zuev, V.S.; Zueva, G.Ya.: Nanodipoles for an optical phased array. J. Russ. Laser Res., **28** (3) (2007), 272.

[14] Li, J.; Engheta, N.: Core-shell nanowire optical antennas fed by slab waveguides. IEEE Trans. Antennas Propag., **55** (11) (2007), 3018.

[15] Kern, A.M.; Martin, O.J.F.: Surface integral formulation for 3D simulations of plasmonic and high permittivity nanostructures. J. Opt. Soc. Am., **26** (4) (2009), 732.

[16] Lerer, A.M.; Makhno, V.V.; Makhno, P.V.; Yachmenov, A.A.: Calculation of periodic metal nanostructures via the method of approximate boundary conditions. J. Commun. Technol. Electron., **52** (4) (2007), 399–405.

[17] Golovacheva, E.V.; Lerer, A.M.; Parkhomenko, N.G.: Diffraction of electromagnetic waves of optical range on a metallic nanovibrator. Moscow Univ. Phys. Bull., **66** (1) (2011), 5–11.

[18] Lerer, A.M.: Investigation of the properties of planar metal nanodipoles in the optical band. J. Commun. Technol. Electron., **56** (3) (2011), 269–277.

[19] Lerer, A.M.; Kleshchenkov, A.B.; Lerer, V.A.; Labun'ko, O.S.: A method for calculation of the characteristics of a system of parallel dipoles excited by stationary and pulse signals. J. Commun. Technol. Electron., **53** (4) (2008), 397–405.

[20] Kravchenko, V.F.; Labunko, O.S.; Lerer, A.M., Sinyavsky, G.P.: Vichislitelnie metodi v sovremennoy radiopfizike. Phizmatlit, Moscow, 2009, 464.

[21] Hiznyak, N.G.: Integralnie urovnenia makroskopicheskoy elektrodinamiki. Naukova Dumka, Kiev, 1986, 279.

[22] http://www.luxpop.com

[23] Makhno, P.V.: Elektrodinamicheskiy analis nanostruktur optichesкogo I rentgenovskogo diapazonov. Dis. Kand. Phys.-Mat Nauk, Rostov-na-Donu, UFU, 2008, 151.

[24] Vainstein, L.A.: Teoria difrakcii I metodi factorizacii. Sovetskoe Radio, Moscow, 1966, 432p.

[25] Lerer, A.M.; Makhno, V.V.; Makhno, P.V.: Calculation of properties of carbon nanotube antennas. Int. J. Microwave Wireless Technol., **2** (6) (2010), 457–462.

[26] Lerer, A.M.; Makhno, V.V.; Makhno, P.V.; Shurov, G.A.: Raschet parametrov nanoanten – uglerodnih nanotrbok. Electromagn. Volni Electro. Sist., **15** (2) (2010), 64–67.

[27] Lerer, A.M.; Makhno, V.V.; Makhno, P.V.: Electrodinamicheskiy analis nanoanten millemetrovogo, opticheskogo i rengenovskogo diapazonov. Lambert Academic Publishing, Saarbrücken, Germany, 2011, 192.

Alexander M. Lerer was born in 1946, Ph.D., Professor of Department of Applied Electrodynamics and Computer Modeling, Physics faculty, Southern Federal University. The areas of scientific interest – high-frequency electrodynamics, mathematical theories of diffraction of electromagnetic waves, mathematical modeling of microwave, THz, optical, and X-ray frequency range devices.

Elena V. Golovacheva received her Ph.D. in 2011 at Southern Federal University. She is now senior lecturer at Department of Applied Electrodynamics and Computer Modeling, Physics faculty, Southern Federal University. The areas of scientific interest – mathematical theories of diffraction of electromagnetic waves, mathematical modeling of microwave, THz, and optical frequency range devices.

Anatoly B. Kleshchenkov received his Ph.D. in 2007 at Southern Federal University. He is now docent at Department of Applied Electrodynamics and Computer Modeling, Physics faculty, Southern Federal University. The areas of scientific interest – development of antennas, mathematical theories of diffraction of electromagnetic waves, modeling of microwave, THz, and optical frequency range devices.

Gennady A. Shurov was born in Kirovograd, Ukraine in 1986. Master of Science in Physics, Southern Federal University (former Rostov State University). Currently, a Ph.D. student. Fields of interest: diffraction of electromagnetic field, antenna design, nanovibrators, carbon nanotubes, nanostructures, and waveguides.

Pavel V. Makhno was born in 1984, Ph.D., docent at Department of Applied Electrodynamics and Computer Modeling, Physics faculty, Southern Federal University. The areas of scientific interest – high-frequency electrodynamics, mathematical theories of diffraction of electromagnetic waves, mathematical modeling of microwave, THz, optical, and X-ray frequency range devices.

Victoria V. Makhno was born in 1980, docent at Department of Informatics and Numerical Experiment of Southern Federal University. The areas of scientific interest – high-frequency electrodynamics, mathematical theories of diffraction of electromagnetic waves, mathematical modeling of microwave, THz, optical, and X-ray frequency range devices.

https://doi.org/10.1017/S1759078713000196 Published online by Cambridge University Press